



Predicting debris-flow clusters under extreme rainstorms: a case study on Hong Kong Island

S. Y. Zhou¹ · L. Gao¹ · L. M. Zhang¹

Received: 27 September 2018 / Accepted: 14 March 2019 / Published online: 4 May 2019
© Springer-Verlag GmbH Germany, part of Springer Nature 2019

Abstract

Debris flows can cause severe loss of human lives and damage to property, especially on densely populated hilly terrains. In the changing climate, the frequency of debris flows is on a rising trend. Therefore, it is important to forecast possible scenarios of debris flows under extreme weather conditions. Previous numerical studies often deal with one individual debris flow in one analysis. Yet a large number of debris flows can occur in a large storm. This paper presents a physically based model to predict likely debris flow clusters on Hong Kong Island with an area of approximately 80 km² considering the influence of the changing climate. Firstly, a slope stability analysis is conducted, and unstable cells and landslide deposition areas are predicted. Then clusters of debris flows initiating from these landslides are simulated considering hillslope erosion. The models are validated with historical debris flows triggered by a rainstorm in 2008. Finally, debris flow clusters under three reference extreme rainstorms (i.e. 44%, 65% and 85% of the 24-h probable maximum precipitation, PMP) are predicted. With the increase of rainstorm magnitude, numerous debris flows can occur simultaneously and merge, posing much greater threat to society. The consequences of debris flows grow dramatically when the magnitude reaches a certain extent, i.e. 65% of the 24-h PMP.

Keywords Debris flows · Landslides · Hillslope erosion · Rainstorms · Natural hazards · Climate change

Introduction

Debris flows have often occurred in clusters under large rain storms (e.g., Staley et al. 2013; Zhang et al. 2013), and caused loss of lives and property. Due to the changing climate, the frequency of extreme storms is becoming larger in Hong Kong and many parts of the world (e.g., Ho 2013; AECOM and Lin 2014), indicating a growing frequency of rainfall-induced landslides and debris flows. For example, the 24-h rainfall intensity of the top 10 outstanding storms in Hong Kong from 1984 to 2010 ranged from 468 mm to 956 mm, while that from 1966 to 1983 ranged from 255 mm to 557 mm (AECOM and Lin 2014). In the future, slope failures can be

more frequent and provide abundant source materials for debris flows. For example, on 7 June 2008, a severe rainstorm hit Hong Kong, triggering 1900 natural terrain landslides, 900 debris flows, and 622 floods (DSD 2008; Li et al. 2009). When many debris flows occur in the same catchment, some of them may merge into a larger debris flow, which can be more catastrophic, especially on Hong Kong Island where the density of population and buildings is very high. While rainfall-induced slope failures have been paid great attention, less effort has been made to analyze debris flow clusters under extreme conditions. An island-wide quantitative assessment of rainfall-induced multiple debris flows under extreme conditions is important to provide a basis for policy-making.

Many qualitative studies on rainfall-induced debris flow clusters have been conducted (e.g. Dai et al. 1999; Chen et al. 2012; Cui et al. 2013; Li et al. 2017; Fan et al. 2018). Dai et al. (1999) investigated the 1993 debris flows on Lantau Island, Hong Kong, conducted field investigations, and carried out laboratory tests to look into the initiation modes of these debris flows. Cui et al. (2013) analyzed 21 simultaneous debris flows induced by rainfall in Qingping Town. Chen et al. (2012) conducted field studies and analyzed the initiation mechanisms and runout characteristics of the rainfall-induced debris flow in Xiaojiagou, Sichuan

✉ L. M. Zhang
cezhangl@ust.hk

S. Y. Zhou
szhouaq@connect.ust.hk

L. Gao
cegaoliang@ust.hk

¹ Department of Civil and Environmental Engineering, The Hong Kong University of Science and Technology, Clearwater Bay, Kowloon, Hong Kong

Province, China. Li et al. (2017) conducted detailed study on the distribution, mobility, and volume changes of the 16 debris flows in mountains near Beijing induced by extreme rainfall on 12 July 2012 by conducting field investigation and aerial photo interpretation. Fan et al. (2018) studied four major debris flow activities in Gaojiagou Ravine during 2010–2016, evaluated the change of loose deposit volumes, and looked into the triggering mechanisms and runout characteristics of these debris flows.

Quantitative studies on debris flows have also been investigated (e.g. Pudasaini 2012; Huang et al. 2015; Gao et al. 2016; He et al. 2016; Han et al. 2017; Bout et al. 2018; Han et al. 2018; Zhang et al. 2018). Pudasaini (2012) proposed a general two-phase debris flow model considering viscous stress, virtual mass, generalized drag, and buoyancy. Huang et al. (2015) simulated the propagation process of post-earthquake debris flows with smoothed particle hydrodynamics (SPH) modelling techniques. Gao et al. (2016) simulated debris flows in an urban catchment on Hong Kong Island. He et al. (2016) proposed a coupled two-phase model to describe the characteristics of debris flow movement. Han et al. (2017) improved a cellular automaton model by proposing a new transition function and regressing the persistence function based on flume tests and studied the run-out extent of the 2010 Yohutagawa debris flow event in Japan. Bout et al. (2018) proposed a two-phase integrated model to simulate landslides, debris flows, and hydrological responses. Han et al. (2018) investigated the runout of a potential debris flow in the Dongwopu gully where the topography is rather complex with a finite volume scheme. Zhang et al. (2018) studied the volume, concentration, discharge, velocity and deposition characteristics of post-seismic debris flows in the Wenchuan earthquake area with a combined soil-water mixing model and depth-integrated particle method. Many numerical models have been developed for debris flow simulation, such as FLO-2D (O'Brien et al. 1993), DAN (Hung 1995), DAN3D (Hung and McDougall 2009), a coupled landslide-debris flow model (Chiang et al. 2012), a basal entrainment model (Ouyang et al. 2015), and EDDA (Chen and Zhang 2015; Shen et al. 2018).

There have been some statistical studies on landslides and debris flows in Hong Kong (e.g. Dai et al. 1999; Ko and Lo 2016) and limited numerical analysis at catchment scale (e.g., Gao et al. 2016); however, the simulation of the burst of debris flow clusters at regional scale is still challenging.

This paper aims to predict potential debris flow clusters over the entire Hong Kong Island under extreme rainfall. In this paper, slope failures under three extreme conditions (i.e. 44%, 65% and 85% of the 24-h probable maximum precipitation, PMP) over the entire Hong Kong Island are simulated first to identify the initiation locations and volumes of debris flows. Then, based on the deposition area and scar area of landslides, two schemes of debris flow simulation are

conducted for debris flows initiating at landslide scars (scheme 1) and at deposition areas (scheme 2). The maximum flow depth and flow velocity of the debris flows under the three extreme storm conditions are predicted, and the flow paths of debris flows are delineated, which provide a basis for debris flow risk management. Finally, the outcomes of the two initiation schemes are compared.

Analysis methodology

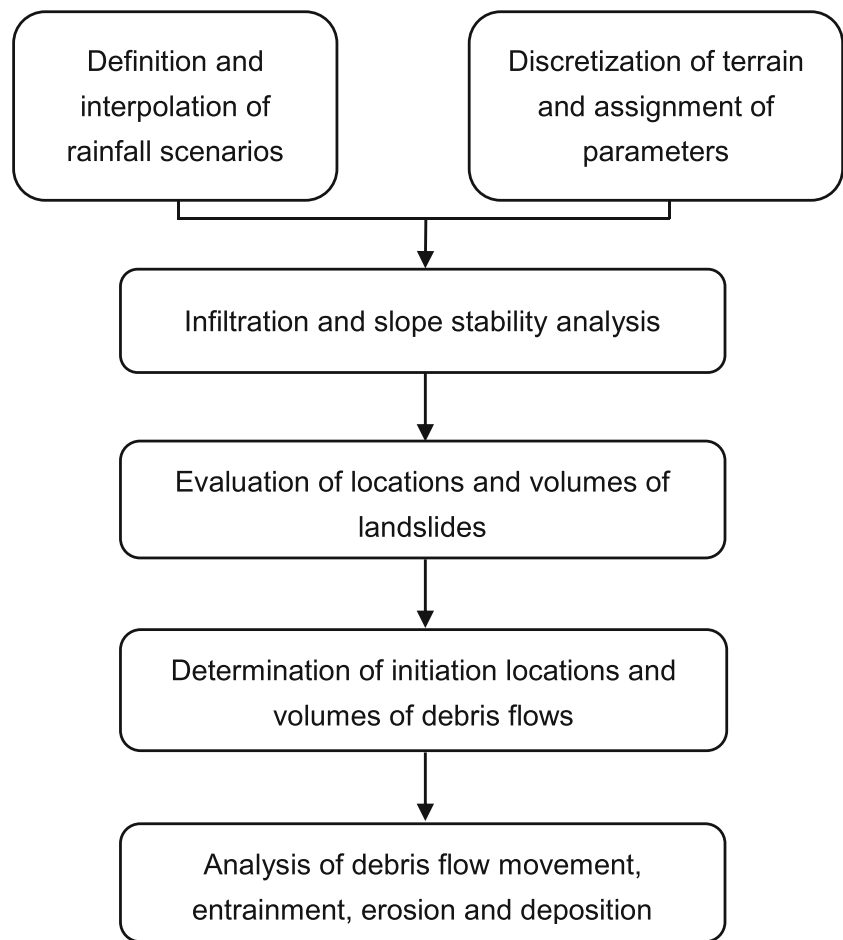
A debris flow can initiate through three mechanisms, e.g. bed erosion, transformation from a landslide, breach of a dam, or combination of processes. Most debris flows in Hong Kong initiated from landslides and bed erosion (e.g. Lam et al. 2012). In this paper, we consider two major debris flow initiation mechanisms simultaneously: transformation from slope failures and bed erosion. As the flow mixture advances, it entrains materials along its flow path by bed erosion. Accordingly, a two-step simulation scheme is adopted (Fig. 1). A slope failure simulation is conducted first to determine the initiation locations and volumes of the debris flows, followed by the simulation of the debris flow movement. The detailed procedure is as follows:

- (a) Discretize the study area into a grid on a digital elevation model (DEM) and assign parameters to each cell such as soil type and material properties.
- (b) Define extreme rainfall scenarios and interpolate the rainfall to the analysis grid.
- (c) Analyze rainfall infiltration, slope stability, and landslide traces to determine the locations and volumes of landslide deposits.
- (d) Determine the initiation locations and volumes of debris flows. The volumes are the sum of the landslide deposits adjacent to each other.
- (e) Analyze the marching, entrainment and deposition process of the debris flows for each scheme.

Initiation locations and volumes of debris flows

Since the main objective of this study is to predict likely debris flows under extreme conditions, the method to simulate shallow slope failures is only presented briefly. More details can be found in Chen and Zhang (2014). Two mechanisms for rainfall-induced slope failures are the rise of pore-water pressure during the process of rainfall infiltration along the interface between the bedrock and the soil where the soil is fully saturated (Collins and Znidarcic 2004), and the loss of shear strength due to the decrease of suction where the soil is unsaturated (Fredlund and Rahardjo 1993; Zhang et al. 2011). To

Fig. 1 Simulation procedure in this study



simulate rainfall-induced slope failures, an infiltration analysis should be conducted first. It is assumed that the soils in this study are homogeneous, and the Richards equation is adopted to describe the infiltration process.

$$\frac{\partial}{\partial z^*} \left(k \frac{\partial \psi}{\partial z^*} \right) + \frac{\partial k}{\partial z^*} \cos \beta = \frac{\partial \theta}{\partial t} \tag{1}$$

where k is the permeability; ψ is the pore-water pressure head; z^* is the layer thickness in the normal direction; β is the slope angle; t is time; θ is the volumetric water content.

The permeability function adopted here is the empirical equation proposed by Gardner (1958):

$$k = k_s e^{\alpha \psi} \tag{2}$$

where k_s is the saturated permeability and α is a material parameter. The soil-water characteristic curve (SWCC) proposed by Gardner (1958) is adopted:

$$\theta = \theta_r + (\theta_s - \theta_r) e^{-\alpha \psi} \tag{3}$$

where θ_s and θ_r are the saturated and residual volumetric water content, respectively.

After the infiltration analysis, the slope stability is evaluated. Since most of the slope failures in Hong Kong are shallow-seated with sliding depths seldom exceeding 3 m (Au 1998), only shallow slope failures will be considered. Due to large calculation demands in such a large area, a simple model, i.e. an infinite slope model, is used here to calculate the factor of safety F_s , which is expressed by Brunsden and Prior (1984) for positive pore-water pressure when the slip surface occurs in the saturated zone:

$$F_s = \frac{\tan \varphi'}{\tan \beta} + \frac{c' - \psi(Z, t) \gamma_w \tan \varphi'}{\gamma_s z' \sin \beta \cos \beta} \tag{4}$$

where β is the slope angle; c' and φ' are the effective cohesion and friction angle, respectively; γ_w and γ_s are the unit weights of water and soil, respectively; $\psi(Z, t)$ is the pore-water pressure head at depth Z and time t .

When the slip surface occurs in the unsaturated zone, the pore-water pressure is negative, and F_s is expressed by Fredlund et al. (1978) as:

$$F_s = \frac{\tan \varphi'_b}{\tan \beta} + \frac{c'_b - \psi(Z, t) \gamma_w \tan \varphi'_b}{\gamma_s z' \sin \beta \cos \beta} \tag{5}$$

where φ_b is the friction angle associated with the matric suction ($u_a - u_w$).

Based on historical data, a logistic regression model was proposed by Corominas (1996) to estimate the trace and travel distance of landslides:

$$\text{Log}(H/L) = -0.047 - 0.085 \log(V) \quad (6)$$

where H is the elevation difference between the initiation and deposition points, L is the distance between the two points, and V ($\times 10^3 \text{ m}^3$) is the landslide volume. This relation is shown to be applicable to Hong Kong (Chen and Zhang 2014).

Initiation schemes of debris flows

This study considers two schemes of initiation points, i.e. at the landslide scar (scheme 1) and the deposition area (scheme 2). The two schemes are shown in Fig. 2. When initiating at a landslide scar, the initiation cells of landslides are found from the landslide study, and a certain percentage of the landslide material is assumed to transform into a debris flow. When initiating at a landslide soil deposition, the landslide material is routed to the deposition location according to Eq. (6). The landslide deposits adjacent to each other are grouped. According to the locations and volumes of the deposits, the initiation point is selected near the largest deposit, and the total volume is the total volume of the deposits. If the deposits belong to the same landslide group (where the unstable cells are bordered upon each other; Chen and Zhang 2015), they are grouped and the volumes are aggregated for debris flow initiation analysis.

Debris flow dynamics, erosion and deposition

In the debris flow simulation, an integrated model EDDA 1.0 developed by Chen and Zhang (2015) is adopted here. The governing equations are depth-integrated mass conservation equations (Eqs. 7 and 8) and momentum conservation equations (Eqs. 9 and 10) as described below:

$$\frac{\partial h}{\partial t} + \frac{\partial(hv_x)}{\partial x} + \frac{\partial(hv_y)}{\partial y} = i[C_{v^*} + (1-C_{v^*})s_b] + A[C_{vA} + (1-C_{vA})s_A] \quad (7)$$

$$\frac{\partial(C_v h)}{\partial t} + \frac{\partial(C_v h v_x)}{\partial x} + \frac{\partial(C_v h v_y)}{\partial y} = iC_{v^*} + AC_{vA} \quad (8)$$

$$\frac{\partial v_x}{\partial t} + v_x \frac{\partial v_x}{\partial x} = g \left[-\text{sgn}(v_x) S_{fx} - \frac{\partial(z_b + h)}{\partial x} \right] - \frac{i[C_{v^*} + (1-C_{v^*})s_b] + A[C_{vA} + (1-C_{vA})s_A]}{h} \quad (9)$$

$$\frac{\partial v_y}{\partial t} + v_y \frac{\partial v_y}{\partial y} = g \left[-\text{sgn}(v_y) S_{fy} - \frac{\partial(z_b + h)}{\partial y} \right] - \frac{i[C_{v^*} + (1-C_{v^*})s_b] + A[C_{vA} + (1-C_{vA})s_A]}{h} \quad (10)$$

where h is the flow depth; t is time; v_x and v_y are the average flow velocities in the x and y directions, respectively; i is the rate of erosion or deposition, which can be expressed as $i = -\partial z_b / \partial t$; A is the entrainment rate; C_{v^*} is the volume fraction of solids in the erodible bed; C_{vA} is the volume fraction of solids in the entrained materials; s_b and s_A are the degrees of saturation in the erodible bed and the entrained materials, respectively; C_v is the volumetric sediment concentration of the mixture; g is the gravitational acceleration; S_{fx} and S_{fy} are the flow resistance slopes in the x and y directions, respectively; z_b is the bed elevation; and the sgn function is used to make sure the direction of resistance is opposite to the flow direction.

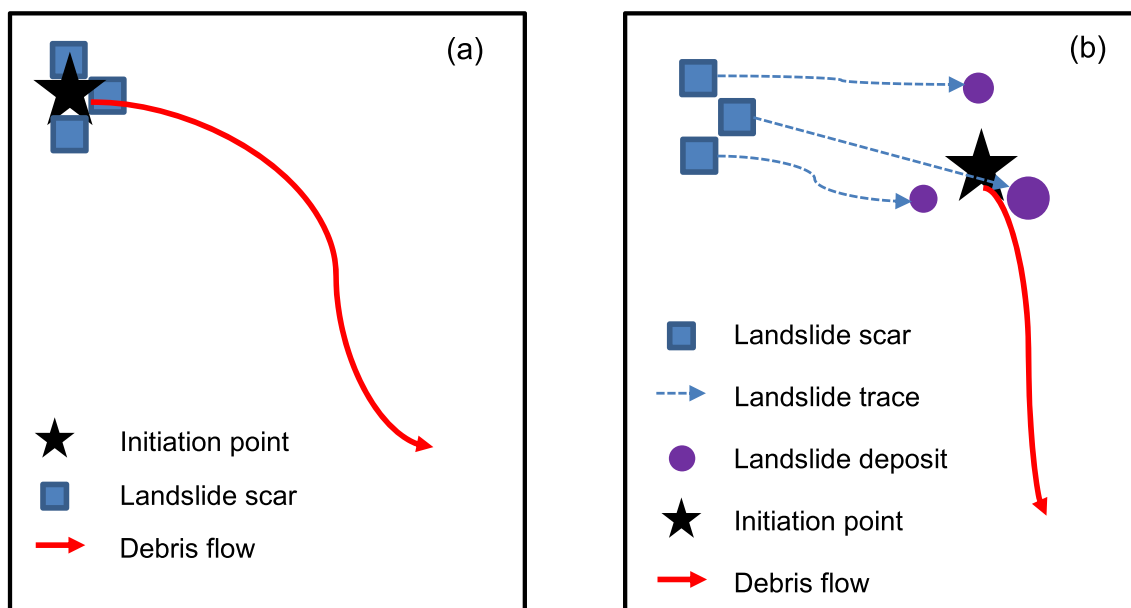


Fig. 2 Two schemes of initiation of debris flow: a at the landslide scar, and b at the landslide deposition area

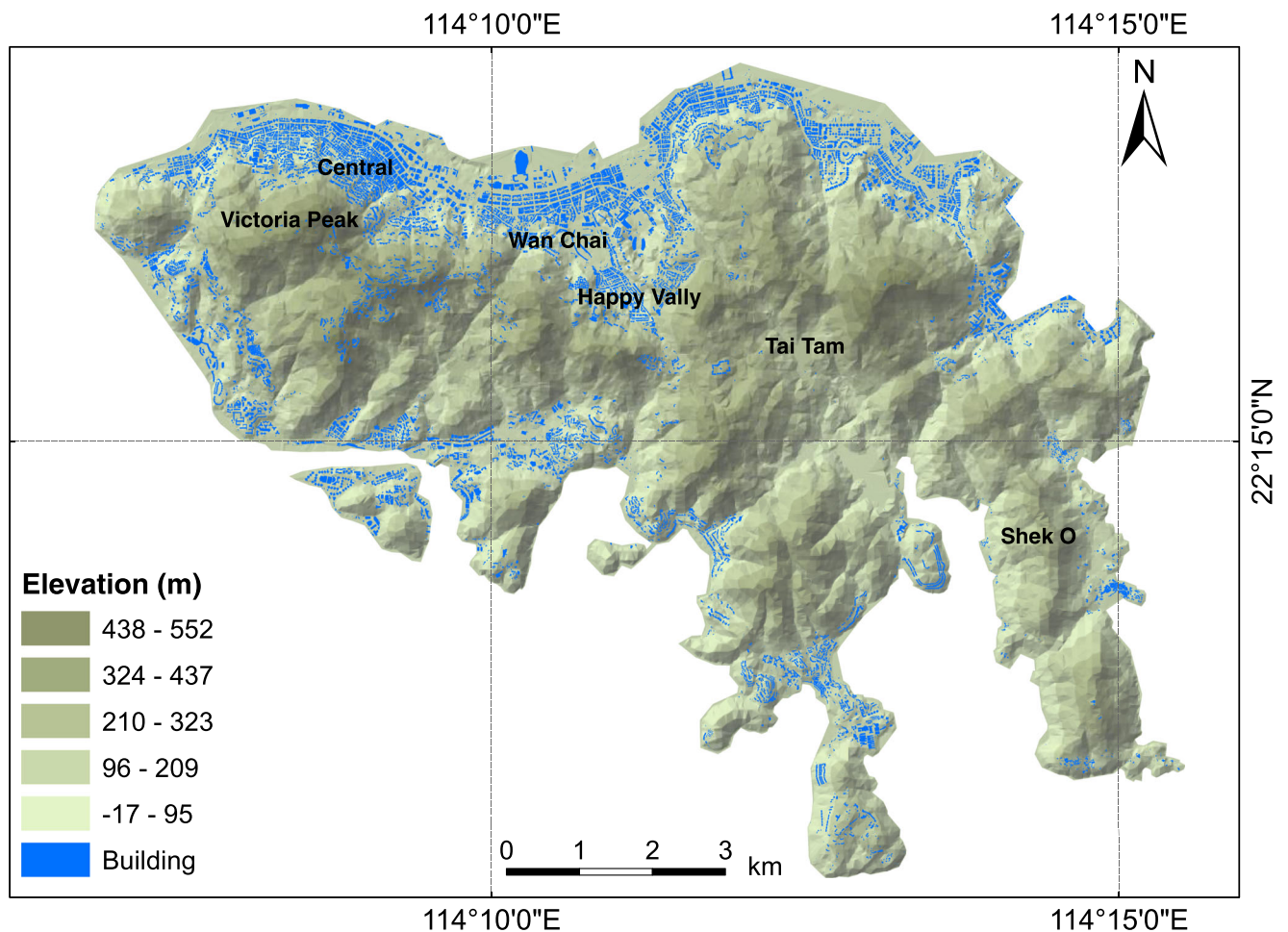


Fig. 3 Ground surface elevations and building distributions on Hong Kong Island

The quadratic rheological model (Julien and Lan 1991), which accounts for friction, viscosity and turbulent flow, is adopted in this study:

$$S_f = \frac{\tau_y}{\rho gh} + \frac{K\mu V}{8\rho gh^2} + \frac{n_{td}^2 V^2}{h^{4/3}} \tag{11}$$

where K is the resistance parameter for laminar flow; μ is the dynamic viscosity; V is average velocity of the mixture; ρ_s and ρ_w are the densities of the solid and water, respectively; n_{td} is the equivalent Manning coefficient which adopts the value recommended by the FLO-2D reference manual (FLO-2D Software Inc. 2009); τ_y is the yield stress of the debris flow.

Empirical equations proposed by O'Brien and Julien (1988) are adopted to estimate the yield stress and dynamic viscosity:

$$\tau_y = \alpha_1 e^{\beta_1 C_v} \tag{12}$$

$$\mu = \alpha_2 e^{\beta_2 C_v} \tag{13}$$

where $\alpha_1, \alpha_2, \beta_1$, and β_2 are empirical coefficients.

Characterization of the erosion and deposition process is essential in debris flow analysis. Erosion occurs when the bed shear stress is sufficiently large and the volumetric sediment concentration of the debris flow mixture C_v is smaller than an equilibrium value proposed by Takahashi et al. (1992):

$$C_{v\infty} = \frac{\rho_w \tan\theta}{(\rho_s - \rho_w)(\tan\phi_{bed} - \tan\theta)} \tag{14}$$

where $C_{v\infty}$ is the equilibrium value, and ϕ_{bed} is the internal friction angle of the erodible bed. From the equation above, when the slope angle becomes larger, $C_{v\infty}$ can be larger than 1 or smaller than 0, in which case no erosion process is considered since the cell is not stable. The erosion rate is expressed by Hanson and Simon (2001) as:

$$i = K_e(\tau - \tau_c) \tag{15}$$

where i is the erosion rate; K_e is the coefficient of erodibility; τ_c is the critical erosive shear stress; and τ is the shear stress expressed by Hanson (1990) as:

$$\tau = \rho gh S_f \tag{16}$$

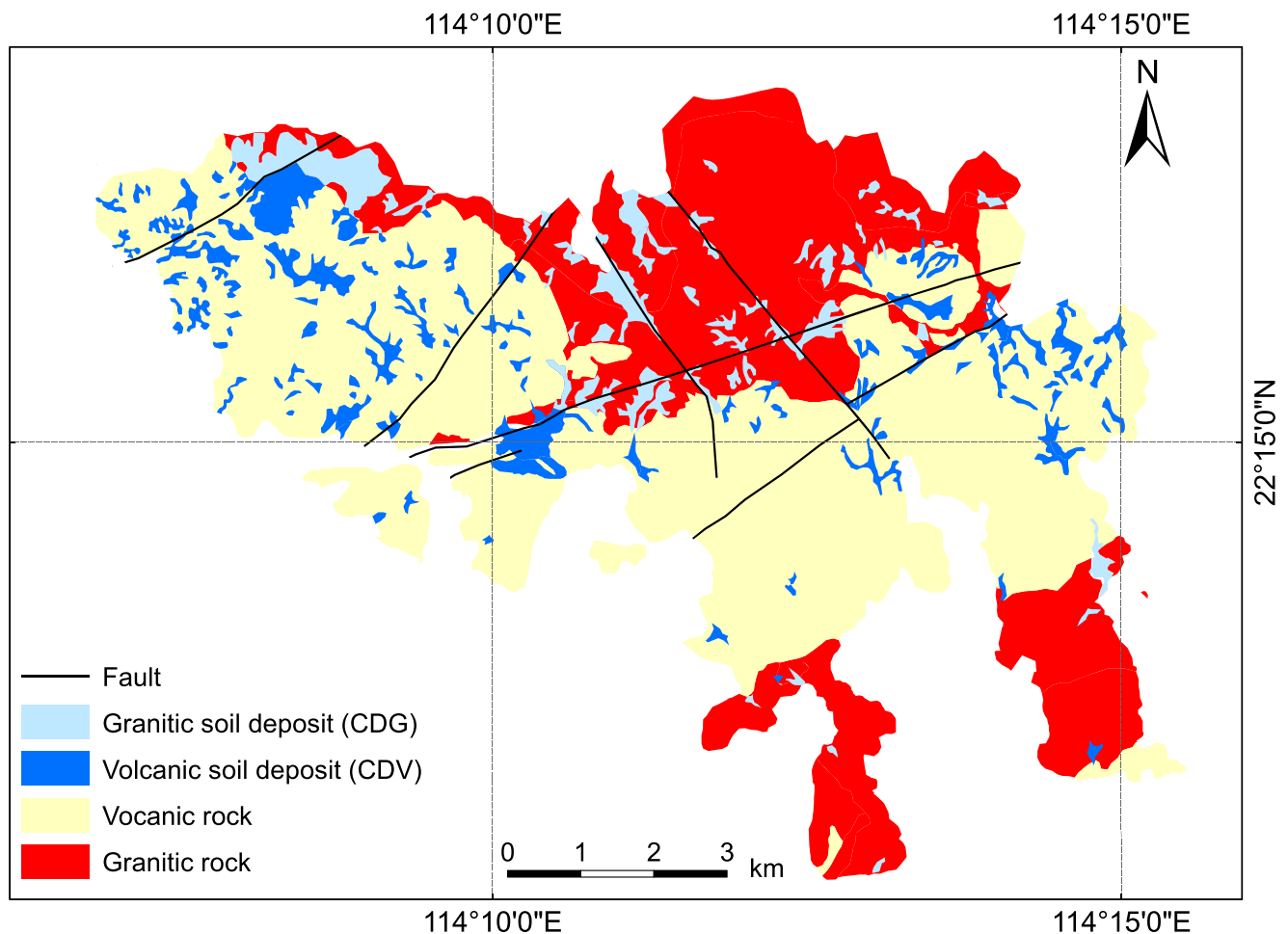


Fig. 4 Bedrock and superficial soil deposits in the study area

When the slope angle is small, C_v can be larger than $C_{v\infty}$ and, hence, deposition of the solid material will occur. The critical velocity is proposed by Takahashi et al. (1992) as follows:

$$V_e = \frac{2}{5d_{50}} \left(\frac{g \sin \theta_e \rho}{0.02 \rho_s} \right)^{0.5} \lambda^{-1} h^{1.5} \quad (17)$$

where d_{50} is the mean particle size and ρ is the density of the mixture.

The rate of deposition can be calculated by (Takahashi et al. 1992):

$$i = \delta_d \left(1 - \frac{V}{pV_e} \right) \frac{C_{v\infty} - C_v}{C_{v*}} V \quad (18)$$

where δ_d is the coefficient of deposition rate and was calibrated by Chen and Zhang (2015); p is a coefficient related to the location difference between the initiation point of deposition and the point where the velocity becomes smaller than the critical velocity, V_e .

Based on this analysis method and results of slope failures mentioned above, debris flows under extreme rainfall conditions can be analyzed further. Through numerical simulations, the flow path, maximum flow velocity, maximum flow depth, and total debris flow volume can be predicted.

Study area and model parameters

Topography and bedrock conditions

The study area covers the entire Hong Kong Island that has an area of 78.59 km². A high-resolution light detection and ranging (LiDAR) digital terrain model (DEM), with vertical accuracy of ± 0.1 m and horizontal accuracy of ± 0.3 m, was converted to raster format on a GIS platform. The peak elevation of the study area is 551.7 m, which is located at Victoria Peak. The terrain of Hong Kong Island is rather hilly, with 30% of the land steeper than 30°. The slope angle within the area ranges from 0 to 67°. The DEM is shown in Fig. 3.

Table 1 Parameters for slope instability and debris flow simulation

Material zone	Granitic deposit	Volcanic deposit	Vegetated bedrock	Hard urban surface	Granitic bedrock	Volcanic bedrock	Reclaimed land
Friction angle related to soil suction, $\varphi_b(^{\circ})$	28	24	–	–	–	–	24.6
Permeability, k_s (m/s)	8×10^{-6}	4×10^{-6}	–	–	2×10^{-7}	9×10^{-7}	2×10^{-6}
Saturated volumetric water content, θ_{sat}	0.5	0.5	–	–	0.2	0.2	0.5
Residual water content, θ_{res}	0.27	0.27	–	–	0.07	0.07	0.27
Material parameter, α	0.7	0.7	–	–	0.7	0.7	0.7
Volume fraction of solids in erodible bed, C_{v*}	0.65	0.65	0.65	–	–	–	–
Coefficient of erodibility, K_e (m ³ /Ns)	10^{-6}	10^{-6}	10^{-7}	–	–	–	–
Mean particle size, d_{50} (mm)	33	33	–	–	–	–	–
Soil density, ρ_s (kg/m ³)	2650	2665	2680	–	–	–	–
Effective cohesion, c' (kPa)	4	4.5	–	–	–	–	10.5
Internal friction angle, $\varphi_{bed} (^{\circ})$	42	36	–	–	–	–	37
Coefficient of deposition rate, δ_d	0.02	0.02	0.02	0.03	–	–	–
Manning's coefficient, n	0.15	0.15	0.08	0.05	–	–	–
Resistance parameter for laminar flow, K	2500	2500	2500	2500	–	–	–
Coefficient of suspension of solid particles, C_s	0.4	0.4	0.4	0.4	–	–	–

The major characteristics of the geology and superficial conditions have been described by Fyfe et al. (2000). The solid geology of Hong Kong Island (Fig. 4) consists primarily of two main types of rocks, i.e. volcanic rocks and granitic rocks, with volcanic rocks covering over 50% of the area and granitic rocks covering over 40%. Granite rocks are mostly located at the northern part of the island, while volcanic rocks are mostly at the southern part and at high elevations. Eight major faults are found in the study area, mostly along a north-east direction, which can affect both the bedrock and superficial deposits.

Superficial geology and model parameters

The superficial deposits can be classified into volcanic deposits and granitic deposits. According to outcomes of a mid-levels study (Geotechnical Control Office 1982), a correlation study between soil thickness and slope angle has been performed by Gao et al. (2015): The soil thickness gently decreases from foothills to steep slopes as the elevation increases. For slopes gentler than 15°, the soil thickness is estimated as 15 m or larger; for slopes steeper than 50°, the thickness is 0; for slopes between 15° and 50°, the thickness decreases with the slope angle:

$$l = -0.43s + 21.43 \quad (19)$$

where l is the soil thickness (m), and s denotes for the slope angle (degree).

The parameters for slope stability analysis have been calibrated by Gao et al. (2015). The mean particle size of debris materials (i.e. granite deposits and volcanic deposits), $d_{50} = 33$ mm, is adjusted from King (2013). The coefficient of suspension of the solid particles, C_s , is assumed according to Chen and Zhang (2015). The soil density ρ_s is measured and summarized in a mid-levels study (Geotechnical Control Office 1982) and listed in Table 1. A set of erosion parameters should be included. According to Chen and Zhang (2015), the volume fraction of solids in erodible bed C_{v*} for granitic deposits, volcanic deposits, and vegetated bedrock is assumed to be 0.65. The coefficient of erodibility K_e is assumed according to the study of Chang et al. (2011). The effective cohesion of bed materials and the internal friction angle of erodible bed φ_{bed} was measured in the mid-levels study (Geotechnical Control Office 1982).

The coefficient of deposition rate δ_d is assumed to be 0.02 for soil deposits and bedrock and 0.03 for a hard urban surface. Manning's coefficient n and resistance parameter for laminar flow K are listed in Table 1 according to FLO-2D Software Inc. (2009).

Validation with historical records

The slope stability analysis over northwestern Hong Kong Island has been validated by Gao et al. (2015). In this paper, the validity of the analysis methods over the entire Hong Kong Island is checked using the 6–7 June 2008 landslide and debris

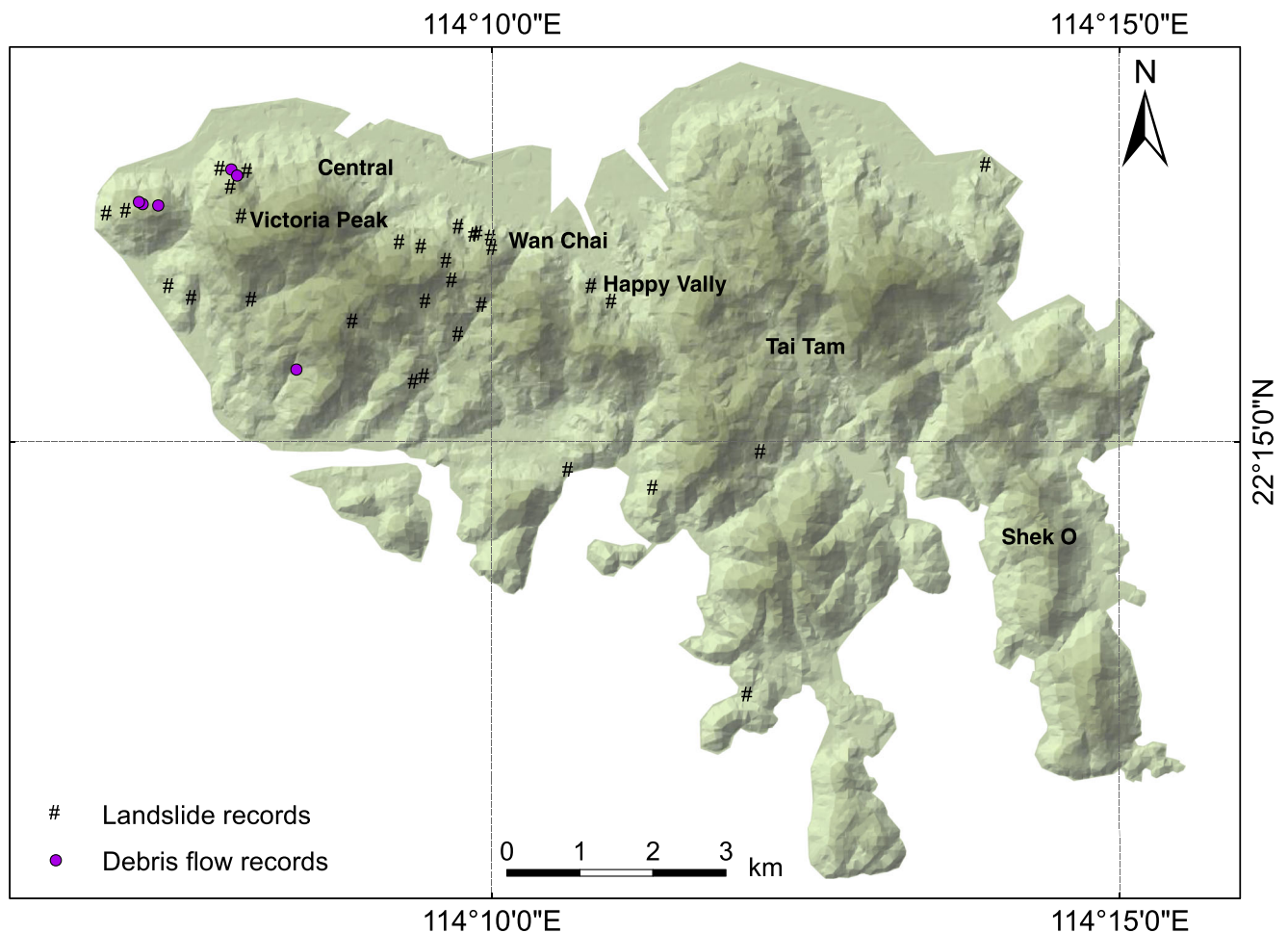


Fig. 5 Slope failures and debris flows in June 2008 under a storm magnitude of 29% of 24-h PMP

flow event. The two schemes of debris flow initiation are examined separately. The rainfall during June 6–7, 2008 corresponded to approximately 29% of the 24-h PMP, and the process was measured using rain gauges and interpolated using universal Kriging over the entire Hong Kong Island.

Slope stability analysis is conducted first to obtain the landslide scars, traces, deposition locations, and volumes, which are key input parameters for debris flow simulation.

During the entire year of 2008, 161 landslide incidents, including 26 major landslides, were recorded on Hong Kong

Table 2 Predicted debris flows under extreme storms for scheme 1 (debris flows initiating at landslide scars)

Magnitude of storm	29% PMP	44% PMP	65% PMP	85% PMP
Landslide volume (m ³)	18,000	57,000	1,124,000	1,838,000
Initial debris volume (m ³)	6000	19,000	371,000	607,000
Maximum travel distance (m)	340	870	1200	1270
Maximum flow depth (m)	2.6	3.8	7.8	8.6
Maximum flow velocity (m/s)	2.7	3.3	5.0	5.0
Total debris flow volume (m ³)	8000	30,000	727,000	1022,000
Deposition volume (m ³)	2000	5000	117,000	179,000
Erosion volume (m ³)	2000	11,000	356,000	415,000
Mobile volume (m ³)	6000	25,000	610,000	843,000
Affected area (m ²)	23,600	111,400	2,610,700	3,214,200
Affected area/terrain area (%)	0.03	0.14	3.32	4.09

PMP probable maximum precipitation

Table 3 Predicted debris flows under extreme storms for scheme 2 (debris flows initiating at deposition areas)

Magnitude of storm	29% PMP	44% PMP	65% PMP	85% PMP
Landslide volume (m ³)	18,000	57,000	1,124,000	1,838,000
Initial debris volume (m ³)	6000	19,000	371,000	607,000
Maximum travel distance (m)	300	680	780	860
Maximum flow depth (m)	2.6	3.7	6.2	6.5
Maximum flow velocity (m/s)	2.7	3.3	3.9	4.3
Total debris flow volume (m ³)	7000	30,000	426,000	669,000
Deposition volume (m ³)	1000	7000	66,000	102,000
Erosion volume (m ³)	1000	11,000	55,000	62,000
Mobile volume (m ³)	6000	23,000	360,000	567,000
Area affected by debris flows (m ²)	13,100	94,400	639,400	817,700
Affected area/terrain area (%)	0.02	0.12	0.81	1.04

PMP probable maximum precipitation

Island (Lam et al. 2012). According to the Enhanced Natural Terrain Landslide Inventory (ENTLI) shown in Fig. 5, there were 37 landslides among which 6 turned into debris flows in 2008 over the entire Hong Kong Island, and most of the landslide locations were within the western part of the island. The total landslide volume is approximately 11,700 m³ from the ENTLI records, while the landslide volume that turned into debris flows is estimated to be 4400 m³. One major debris flow occurred on the natural hillside at Mount Davis, and the total initial volume is estimated to be 435 m³. However, some small landslides and debris flows that occurred in remote areas were not recorded, so that the total landslide volume might be underestimated.

According to Zhang et al. (2014) and Zhang and Zhang (2017), the proportion of loose deposits that turned into debris flows in active catchments during storms at Wenchuan earthquake area in 2010 was 24.5%. Hence, the assumption adopted in this study that 1/3 of the total landslide volume is transformed into debris flow is slightly on the safe side. The calculated total landslide volume is 18,000 m³, and the assumed initiation volume is 6000 m³, which is slightly larger than that from the ENTLI records. From Table 2, when initiating at landslide scars, the total volume of the debris flows is 8000 m³, with an erosion volume of 2000 m³. The maximum travel distance is 340 m, while the actual maximum travel distance record in ENTLI records is 344 m. The maximum flow depth, the maximum flow velocity, and the total area that is affected by the debris flows are listed in Table 2 for initiation scheme 1 and Table 3 for initiation scheme 2. When initiating at the deposition areas, the total volume of debris flows is 7000 m³, with an erosion volume of 1000 m³.

From the summary above, it can be noticed that the total volume of debris flows in scheme 1 is larger than that in scheme 2, because the initiation points in scheme 1 are mostly located on hillslopes at higher elevations, while those in scheme 2 are mostly located in valleys at lower elevations.

This also accounts for the difference in the maximum travel distances in the two schemes and the areas affected by debris flows. Hence, the consequences are much more severe if the debris flows initiate at the landslide scars.

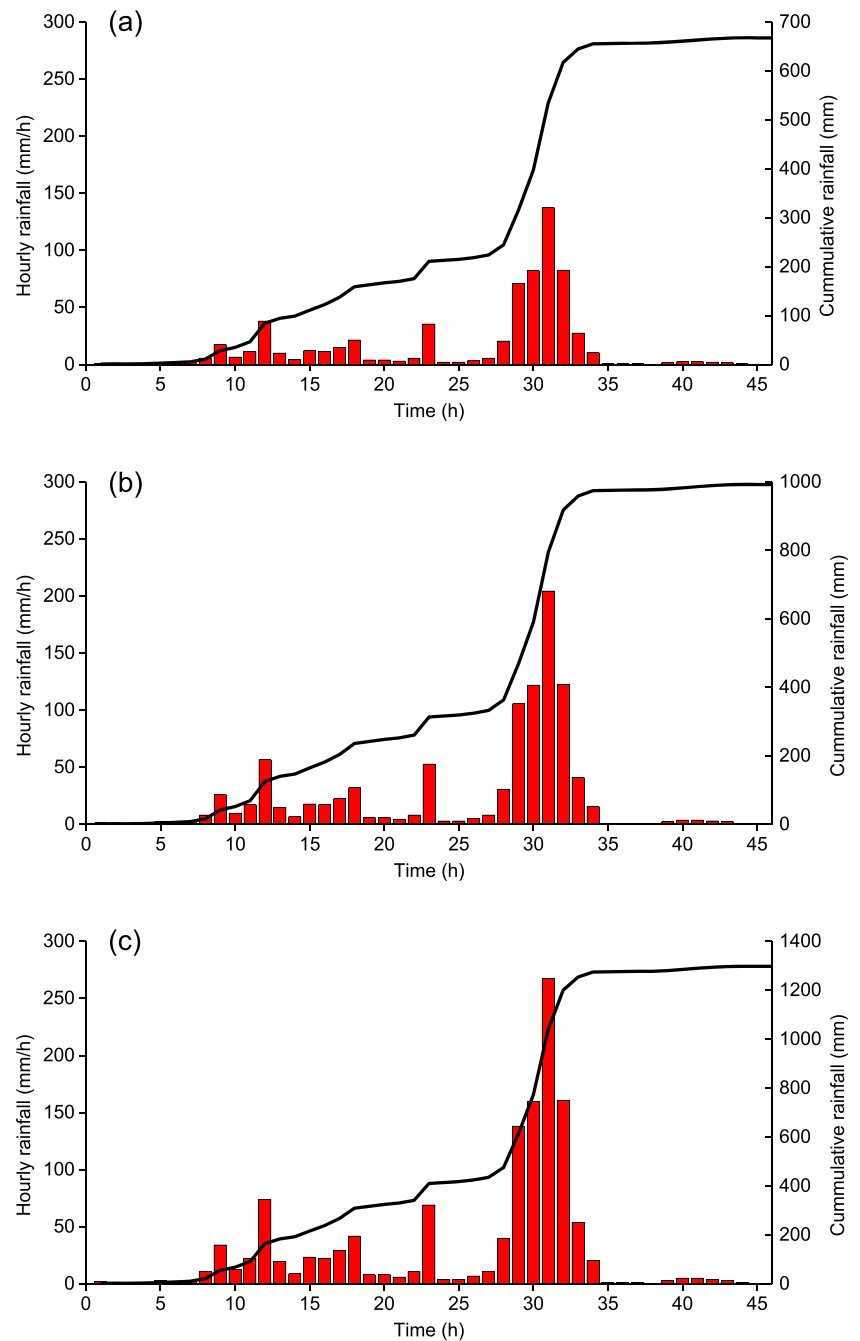
The assumed initiation volume is slightly overestimated for several reasons. First, many small landslides were not recorded in the database because they occurred at remote areas or their volumes were too small to be recorded. Second, the initial volume is estimated from landslide scars, and the debris flow records in the ENTLI include channelized debris flows only. Third, only natural terrain slope failures are considered in the study.

Prediction of likely debris flow clusters under extreme storms

Probable maximum precipitation (PMP) is used to represent the magnitude of a storm, especially for extreme rainfall (WMO 2009). The rainfall on 6–7 June 2008 was adopted as a reference storm for the validation and verification of the analysis methods in this study. According to Chang and Hui (2001), the maximum rolling 24-h rainfall of this storm on Hong Kong Island corresponds to approximately 29% PMP.

Three additional scenarios of extreme rainstorms corresponding to 44%, 65% and 85% of the 24-h PMP are generated for predicting future scenarios of debris flows on Hong Kong Island. The rainfall is assumed to be uniformly distributed over the entire island in this study. The rainfall data is from the record at rain gauge N19 on Lan Tau Island, and the record at this gauge corresponds to 44% of the 24-h PMP, with a total rainfall of 668 mm. The rainfall data at this rain gauge is then upscaled to 65% and 85% of the 24-h PMP by applying suitable upscaling factors (Gao et al. 2015). A storm of 65% of the 24-h PMP corresponds to the maximum rainfall in the history of Hong Kong (Chang and Hui 2001) with a total

Fig. 6 Hyetographs of a 44%, b 65%, and c 85% of 24-h PMP



rainfall of 982 mm. A storm of 85% PMP is an extremely rare case considering the local moisture maximization, with a total rainfall of 1290 mm. The hyetographs are shown in Fig. 6. The influence of the spatial distribution of rainfall is not considered in this study.

From the prediction of the slope failures, the total soil deposit volumes are $57 \times 10^3 \text{ m}^3$, $1124 \times 10^3 \text{ m}^3$ and $1838 \times 10^3 \text{ m}^3$ under 44%, 65% and 85% of the 24-h PMP, respectively. With the assumption that 1/3 of the total volume of landslide deposits is transformed into debris flows, the initiation debris flow volumes are assumed to be $19 \times 10^3 \text{ m}^3$, $371 \times 10^3 \text{ m}^3$ and

$607 \times 10^3 \text{ m}^3$, respectively. Based on the simulation results of slope failures and the assumptions mentioned above, the predicted debris flows initiating at the landslide scars and deposition areas are listed in Tables 2 and 3, respectively. The landslide deposits and landslide scars are presented in Fig. 7. The distributions of the maximum flow depth and velocity for scheme 1 are presented in Figs. 8 and 9, respectively.

Figure 10 shows how the urban area at the central area is affected by debris flow clusters under different storm magnitudes. At 44% of the 24-h PMP, only 1 debris flow occurs in the catchment, and the runout distance is relatively small. The

Fig. 7 Simulation results of landslide deposits and landslide scars corresponding to a 44%, b 65%, and c 85% of 24-h PMP

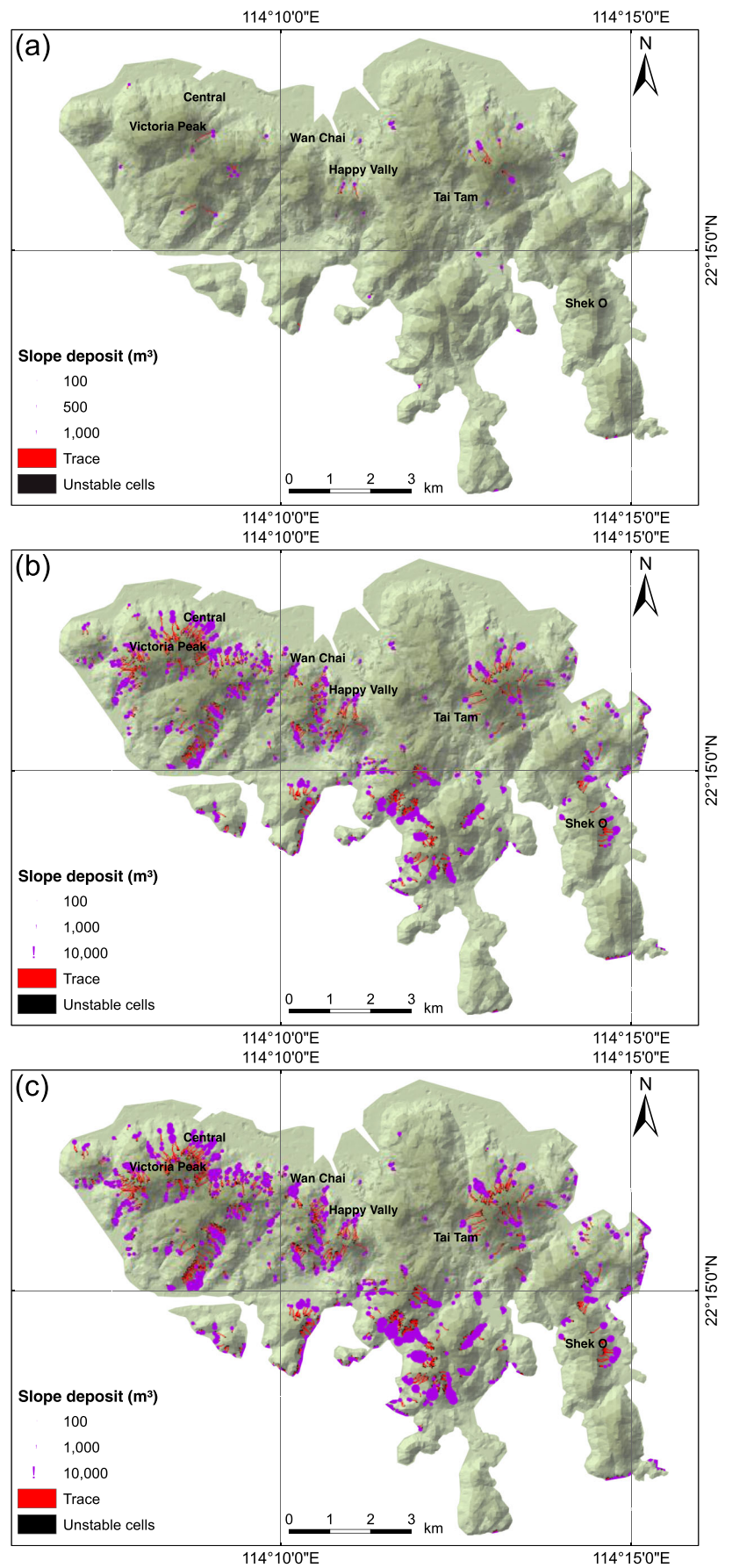


Fig. 8 Simulation results of maximum debris flow depth corresponding to a 44%, b 65%, and c 85% of 24-h PMP for scheme 1 in which debris flows are initiated at landslide scars

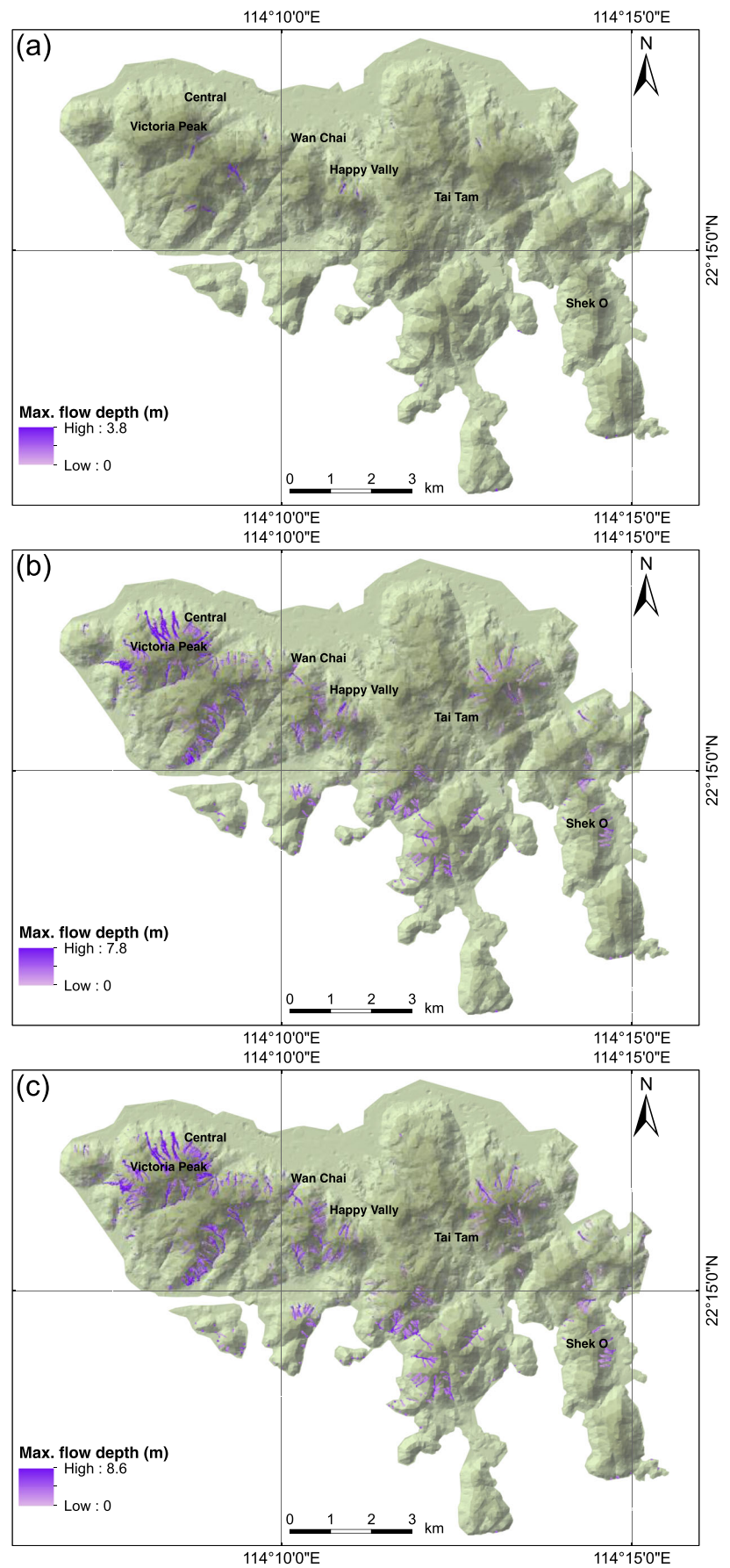


Fig. 9 Simulation results of maximum debris flow velocity corresponding to a 44%, b 65%, and c 85% of 24-h PMP for scheme 1 in which debris flows are initiated at landslide scars

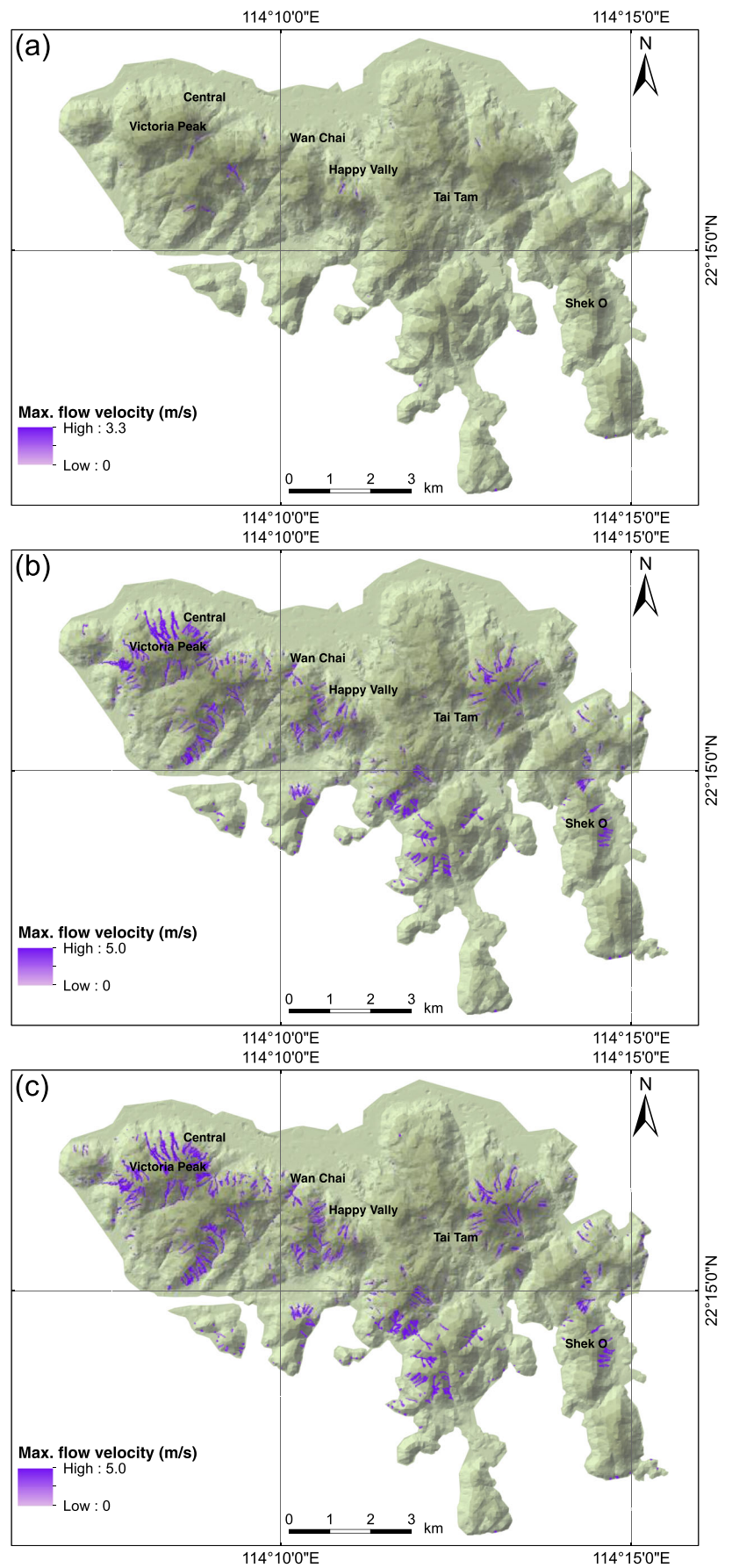
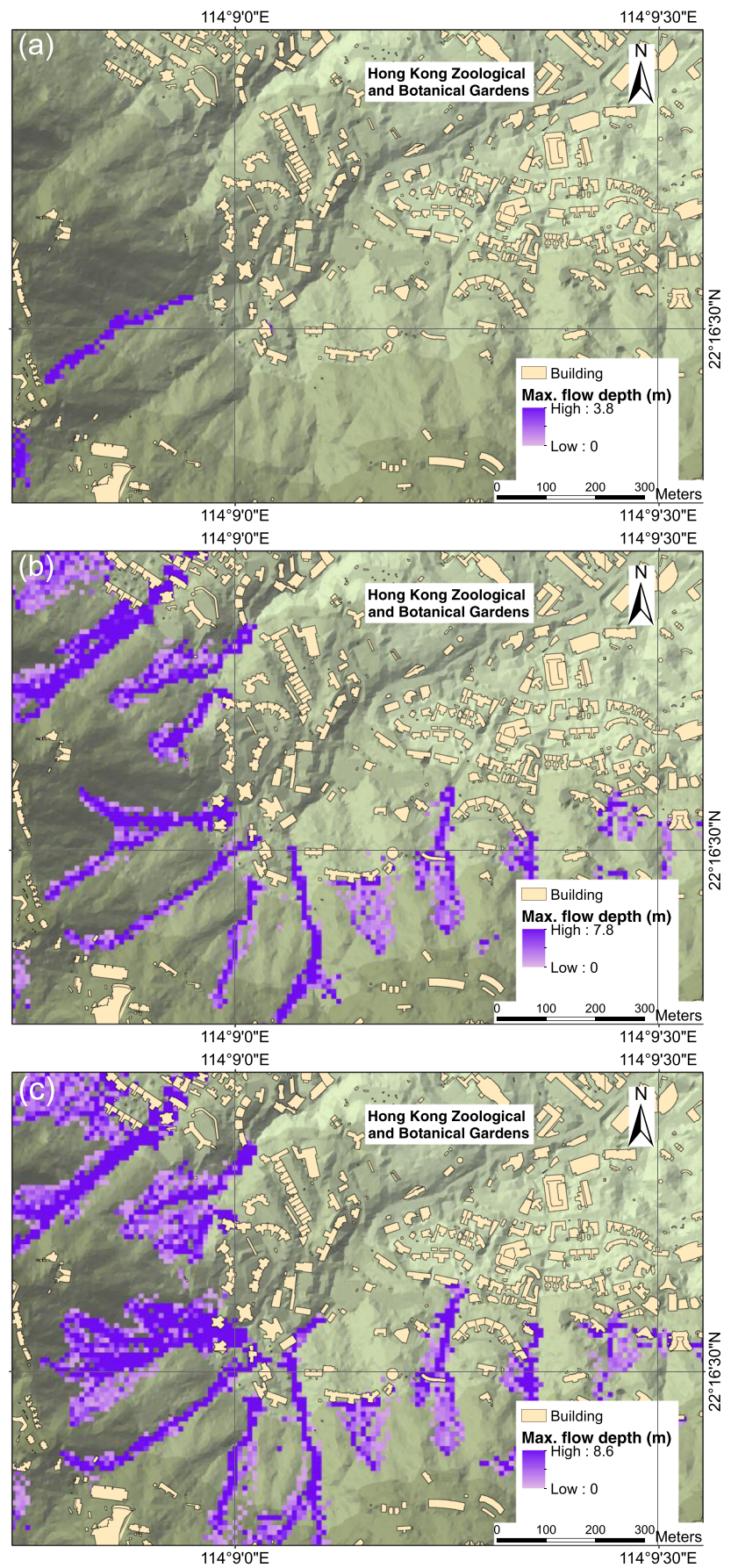


Fig. 10 Simulation results of maximum debris flow depth at the central area corresponding to a 44%, b 65%, and c 85% of 24-h PMP for scheme 1 in which debris flows are initiated at landslide scars



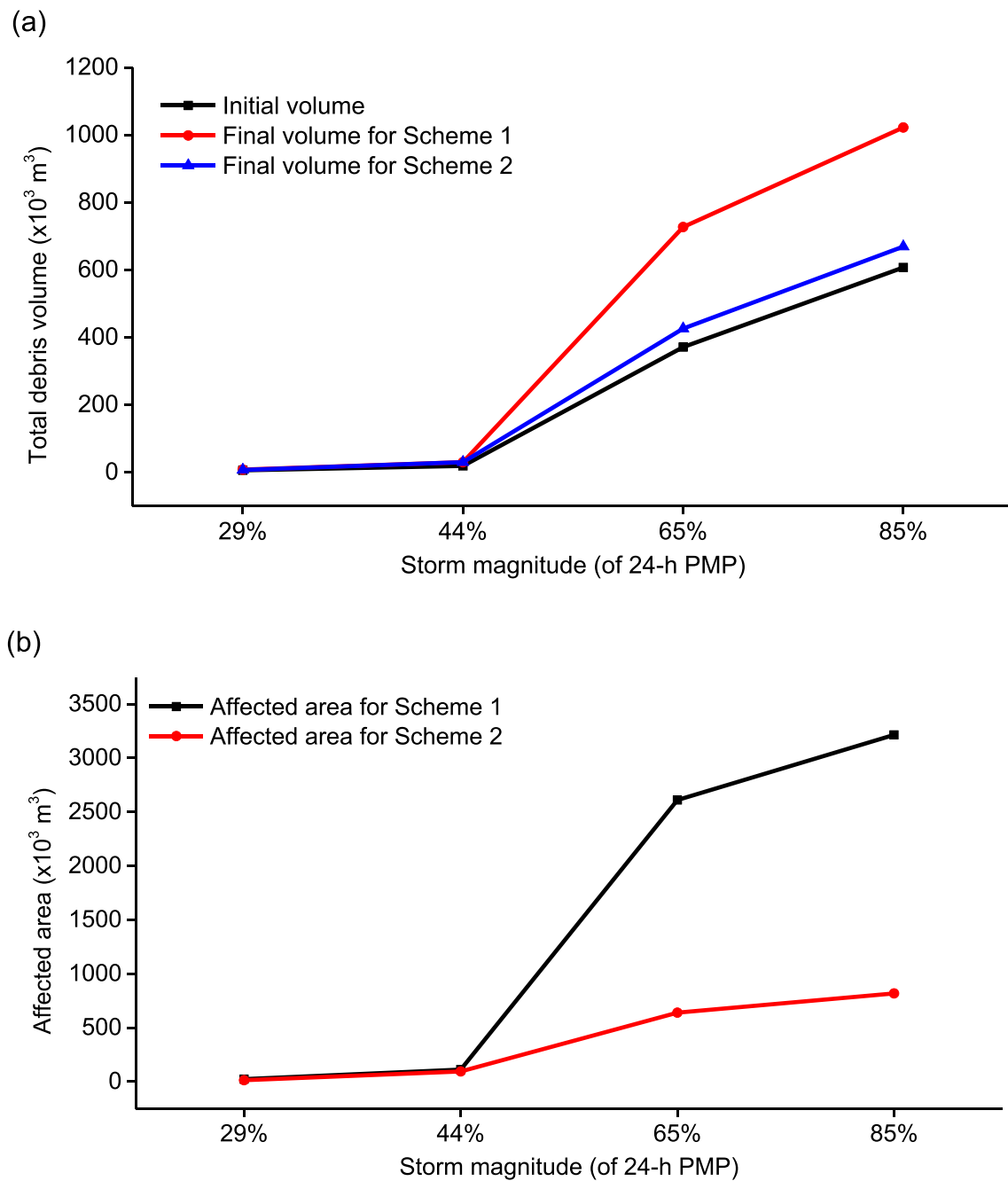


Fig. 11 Comparison of a debris flow volumes and b affected areas under different storm magnitudes for scheme 1 in which debris flows are initiated at landslide scars and scheme 2 in which debris flows are initiated at landslide deposition areas

debris flow stops at the foot of the hill and no building is affected. When the storm magnitude increases to 65% of the 24-h PMP, a lot of debris flows are initiated in the catchment, and some buildings closest to the foot of the hill are affected by debris flows. When the storm magnitude reaches 85% of the 24-h PMP, the number of debris flows does not grow much, but the magnitude of debris flows increases significantly. Some debris flows even run further into the urban area. A large number of buildings and people in the area can be affected.

For the debris flows that initiate at the landslide scars, as shown in Table 2, the total volumes reach $30 \times 10^3 \text{ m}^3$, $727 \times 10^3 \text{ m}^3$, and $1022 \times 10^3 \text{ m}^3$, respectively, in the three storm scenarios. The erosion volumes are $11 \times 10^3 \text{ m}^3$, $356 \times 10^3 \text{ m}^3$, and $415 \times 10^3 \text{ m}^3$, respectively. The large entrained soil volumes agree well with common observations that entrainment is a significant factor in debris flow development. The areas that are affected by debris flows are $111.4 \times 10^3 \text{ m}^2$, $2610.7 \times 10^3 \text{ m}^2$, and $3214.2 \times 10^3 \text{ m}^2$, respectively. For the debris flows that initiate at the deposition areas (Table 3), the

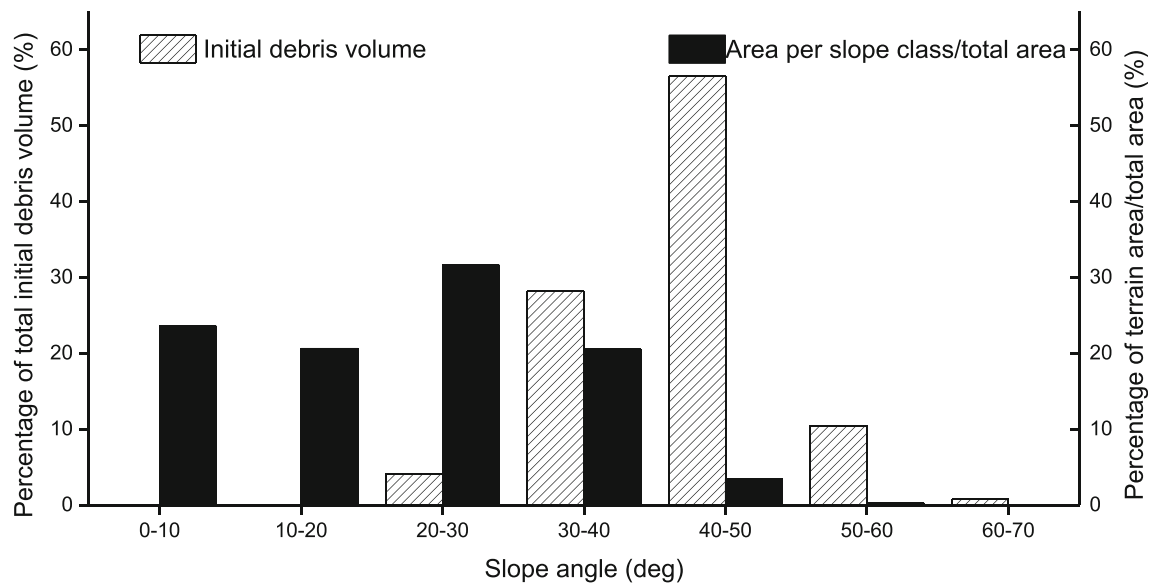


Fig. 12 Influence of slope angle on initial debris volume under a storm of 85% of PMP

total volumes of debris flows reach $30 \times 10^3 \text{ m}^3$, $426 \times 10^3 \text{ m}^3$, and $669 \times 10^3 \text{ m}^3$, respectively. The areas affected by the debris flows are $94.4 \times 10^3 \text{ m}^2$, $639.4 \times 10^3 \text{ m}^2$, and $817.7 \times 10^3 \text{ m}^2$, respectively. Figure 11 compares the debris flow volumes and affected areas in the two initiation schemes.

As shown in the figures and tables, the consequences in scheme 1 are much more severe than those in scheme 2. The area of debris flow path is much larger in the first scheme. The total volumes in scheme 1 are 1.0, 1.7, and 1.6 times those in scheme 2, and the maximum flow depth and maximum flow velocity are also larger. Thus, the debris flows in scheme 1 can be more destructive. Within each scheme, the maximum flow velocity, flow depth, travel distance, total volume of debris flow, and area affected increase with the initial debris volume or the magnitude of rainstorm. The differences between the consequences of those under 44% PMP and those under 65% PMP are much larger than the differences between those under 65% PMP and 85% PMP, which means the debris flow scale grows dramatically when the storm magnitude increases from

44% to 65% PMP, while the growth becomes slower when the storm magnitude is even larger. From the results, it can be inferred that a threshold has probably been reached when the storm magnitude grows up to 65% of the 24-h PMP. Taking the total debris flow volumes in scheme 1 as an example, the total debris volume under 65% PMP is 24 times that under 44% PMP, while that under 85% PMP is only 1.4 times that under 65% PMP. The erosion volumes in scheme 1 also grow dramatically with the initial debris volume. Thus, the hazard intensities in scheme 1 are much higher than those in scheme 2.

There are two reasons for the different consequences in the two schemes. First, the initiation locations in scheme 2 are at deposition zones, which are at low elevations and the slope angles are smaller. Thus the erosion rate is smaller according to Eq. (15). Second, when initiating at the landslide scars, the flow paths of debris flows are longer than those in scheme 2, which also means a larger amount of entrainment. In scheme 1, the debris flows are assumed to initiate at the landslide scars

Table 4 Predicted debris flows under extreme storms under 65% of PMP considering different transformation rates for scheme 1 (debris flows initiating at landslide scars)

Transformation ratio	33%	50%	100%
Initial debris volume (m^3)	371,000	562,000	1,124,000
Maximum travel distance (m)	1200	1280	1500
Maximum flow depth (m)	7.8	9.0	10.9
Maximum flow velocity (m/s)	5.1	5.2	5.8
Total debris flow volume (m^3)	727,000	992,000	1,710,000
Deposition volume (m^3)	117,000	172,000	335,000
Erosion volume (m^3)	356,000	430,000	586,000
Mobile volume (m^3)	610,000	820,000	1,375,000
Area affected by debris flows (m^2)	2,610,700	2,958,400	3,610,700

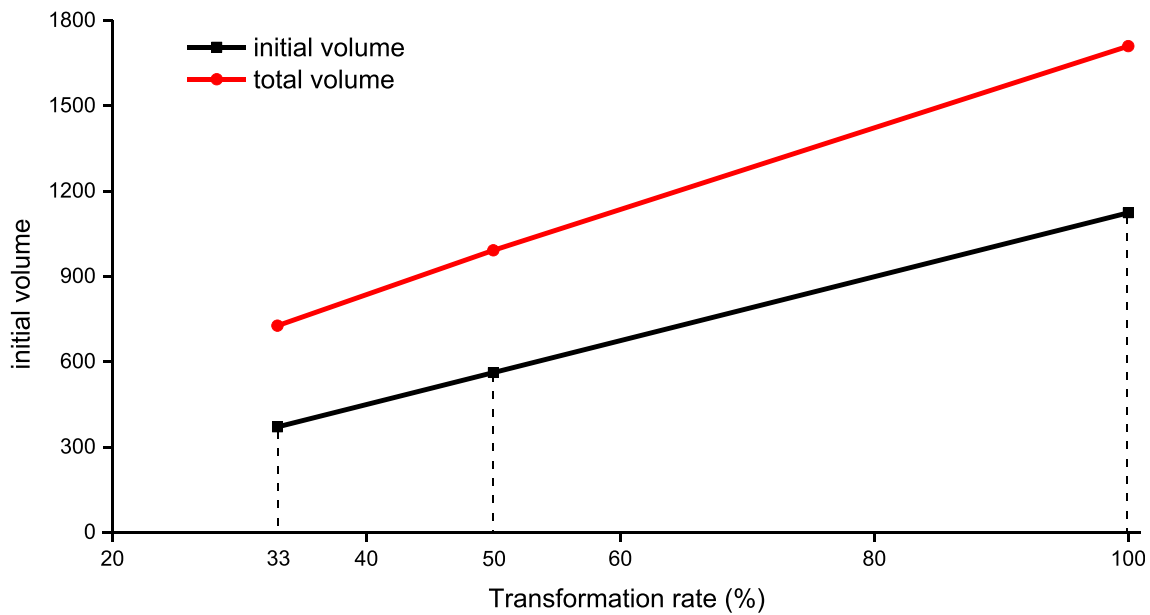


Fig. 13 Comparison of initial debris volume and total debris flow volume corresponding to different transformation rates under a storm of 65% of PMP

and the landslide scars with the highest elevations are almost the same under the three rainstorms. According to Figs. 8 and 9, the debris flows can reach the urban area more easily under extreme conditions, which poses a great threat to society, and have to be prepared for.

Key factors influencing the magnitude of debris flow clusters

Influence of slope angle

A parametric study is conducted to examine the influence of the slope angle at the initiation point on the results. Figure 12 shows the percentage of total initial debris volume vs. slope angle for 85% of the 24-h PMP and the distribution of slope angle of the terrain. The figure shows

Table 5 Predicted debris flows under an extreme storm of 65% PMP considering different effective cohesion values (scheme 1, debris flows initiating at landslide scars)

Effective cohesion (kPa)	3.5	4.0/4.5	5.5
Initial debris volume (m ³)	690,000	371,000	10,000
Maximum travel distance (m)	1250	1200	750
Maximum flow depth (m)	9.4	7.8	4.5
Maximum flow velocity (m/s)	5.2	5.1	3.8
Total debris flow volume (m ³)	1,183,000	727,000	21,000
Deposition volume (m ³)	221,000	117,000	5000
Erosion volume (m ³)	493,000	356,000	11,000
Mobile volume (m ³)	962,000	610,000	16,000
Area affected by debris flows (m ²)	3,080,900	2,610,700	6300

that the terrain is rather steep and about 30% of the terrain area is steeper than 30°. No debris flow initiates in areas with slope angles gentler than 20°. The majority of debris flows initiate at slopes ranging from 30° to 50°. The total initial debris flow volume is the largest on slopes ranging from 40° to 50° in this case, which means that this range is the most susceptible to debris flows and should be paid more attention when taking actions to cope with slope failures and debris flows.

Influence of initial debris volume

A sensitivity study is conducted to study the fraction of the volume that turns into a debris flow from a soil deposit. In this section, the 65% PMP is selected as a study storm case. In addition to a transformation rate of 33% that is assumed in the previous section, transformation rates of 50% and 100% are examined in this section, which are obviously on the safe side. The simulation results are listed in Table 4. The assumed total initial debris volumes are $562 \times 10^3 \text{ m}^3$ and $1124 \times 10^3 \text{ m}^3$. The total volumes of the debris flows increase from $727 \times 10^3 \text{ m}^3$ for a transformation ratio of 33% to $992 \times 10^3 \text{ m}^3$ and $1710 \times 10^3 \text{ m}^3$ for transformation ratios of 50% and 100%, respectively. The affected area increases from $2610.7 \times 10^3 \text{ m}^2$ to $2958.4 \times 10^3 \text{ m}^2$ and to $3610.7 \times 10^3 \text{ m}^2$, respectively. A comparison of the initial and total debris flow volumes is presented in Fig. 13. The total debris flow volume grows approximately proportional to the initial volume. From Table 4, it can be found that the travel distance, total volume, erosion volume, mobile volume, maximum flow depth and velocity, and affected area all increase as the initial debris volume increases.

Influence of effective cohesion

A sensitivity study is conducted to study the influence of the effective cohesion of soil. In this section, the 65% PMP storm [Fig. 6(b)] is selected as a reference storm, and the landslide transformation rate is assumed to be 33%. In addition to the values of 4.5 kPa for volcanic deposits and 4.0 kPa for granitic deposits, effective cohesion values of 3.5 kPa and 5.5 kPa for both types of deposits are examined in this section. The simulation results are listed in Table 5. The total initial debris flow volumes are obtained as $690 \times 10^3 \text{ m}^3$ and $10 \times 10^3 \text{ m}^3$ for 3.5 kPa and 5.5 kPa, respectively; the total volumes of debris flows are $1183 \times 10^3 \text{ m}^3$ and $21 \times 10^3 \text{ m}^3$, respectively, and the affected areas are $3080.9 \times 10^3 \text{ m}^2$ and $6.3 \times 10^3 \text{ m}^2$ for 3.5 kPa and 5.5 kPa, respectively. It can be found that the effective cohesion has a great influence on the hazard magnitudes. This is expected, as cohesion is a controlling factor for shallow-seated failures. The cohesion of fully saturated grade IV or grade VI granitic or volcanic deposits is zero. The presence of small cohesion reflects the contributions of vegetation roots and the soil suction that is not completely dissipated during rainfall infiltration (e.g. Zhu and Zhang 2015; Zhu et al. 2017). Both factors are known to help prevent shallow-seated slides.

Limitations

The models in this study are subject to several limitations:

- (1) The geological and initial conditions (e.g. the initial water table) for all analysis cases are assumed to be the same in this study, while they may vary under different rainfall scenarios.
- (2) Each type of material is considered to be isotropic and homogeneous. The parameters of soils can vary due to their spatial distributions and histories, especially in such a large area as the entire Hong Kong Island. The variation in each soil type is not considered; for example, granitic colluvium and granitic alluvium are both classified as completely decomposed granite (CDG).
- (3) The study follows a two-step analysis procedure, which means slope failure and debris flow simulations are conducted separately. The initiation points of debris flows are identified from the slope failure simulation results. Thus, an integrated full-process analysis that takes surface runoff and groundwater flow, and landslides and

debris flows as a single process will be preferred in the future.

Conclusions

Possible clusters of debris flows over the entire Hong Kong Island under extreme rainstorm conditions have been studied in this paper. In addition to a physically based distributed cell model adopted in the slope failure analysis, a depth-integrated computational scheme considering erosion and deposition processes is adopted to predict likely debris flows. The models are validated using historical records of the rainstorm during 6–7 June 2008. Finally, the debris flows under three extreme rainfall scenarios, i.e. 44%, 65%, and 85% of the 24-h PMP, are predicted. Based on the study, the following conclusions can be drawn:

- (1) Under the three extreme rainstorm scenarios, 0.14%–4.09% of the Hong Kong Island can be affected by debris flow clusters when they initiate at the landslide scars, and 0.12%–1.04% when they initiate at the landslide deposition areas.
- (2) The travel distance, maximum flow depth and velocity, total volume, and affected area become much larger with the increase of the storm magnitude, and the consequences when initiating at the landslide scars are much more severe than those when initiating at the deposition areas, as the elevations of the landslide scars are higher.
- (3) The majority of debris flows occur on steep terrains 40° – 50° in slope angle, although such steep terrain only accounts for 3.5% of the land area.
- (4) The sensitivity study shows that when initiating at the same location, the total debris flow volume grows proportionally to the initial debris volume. Therefore, the debris flow scale depends on both the initiation location and the initial volume.
- (5) The total debris flow volume increases 24 times in scheme 1 when the storm magnitude increases from 44% PMP to 65% PMP, but the debris flow scale only increases 1.4 times when the storm magnitude further increases from 65% PMP to 85% PMP.

Acknowledgements The authors acknowledge the support from the Research Grants Council of the Hong Kong SAR (no. C6012-15G and no. 16206217).

References

- AECOM Asia Company Limited, Lin BZ (2014) 24-hour PMP updating study, Agreement No. CE 13/2011 (GE). Geotechnical Engineering Office, Civil Engineering and Development Department, Hong Kong
- Au SWC (1998) Rain-induced slope instability in Hong Kong. *Eng Geol* 51(1):1–36
- Bout B, Lombardo L, van Westen CJ, Jetten VG (2018) Integration of two-phase solid fluid equations in a catchment model for flashfloods, debris flows and shallow slope failures. *Environ Model Softw* 105:1–16
- Brunsdon D, Prior DB (1984) *Slope instability*. Wiley, Chichester
- Chang DS, Zhang LM, Xu Y, Huang RQ (2011) Field testing of erodibility of two landslide dams triggered by the 12 May Wenchuan earthquake. *Landslides* 8(3):321–332
- Chang WL, Hui TW (2001) Probable maximum precipitation for Hong Kong. ATC3 Workshop on rain-induced landslides, Hong Kong
- Chen HX, Zhang LM, Chang DS, Zhang S (2012) Mechanisms and runoff characteristics of the rainfall-triggered debris flow in Xiaojiagou in Sichuan Province, China. *Nat Hazards* 62(3):1037–1057
- Chen HX, Zhang LM (2014) A physically-based distributed cell model for predicting regional rainfall-induced shallow slope failures. *Eng Geol* 176:79–92
- Chen HX, Zhang LM (2015) EDDA 1.0: integrated simulation of debris flow erosion, deposition and property changes. *Geosci Model Dev* 8(3):829–844
- Chiang SH, Chang KT, Mondini AC, Tsai BW, Chen CY (2012) Simulation of event-based landslides and debris flows at watershed level. *Geomorphology* 138(1):306–318
- Collins BD, Znidarcic D (2004) Stability analyses of rainfall induced landslides. *J Geotech Geoenviron Eng* 130(4):362–372
- Corominas J (1996) The angle of reach as a mobility index for small and large landslides. *Can Geotech J* 33(2):260–271
- Cui P, Zou Q, Xiang LZ, Zeng C (2013) Risk assessment of simultaneous debris flows in mountain townships. *Prog Phys Geogr* 37(4):516–542
- Dai FC, Lee CF, Wang SJ (1999) Analysis of rainstorm-induced slide-debris flows on natural terrain of Lantau Island, Hong Kong. *Eng Geol* 51(4):279–290
- Drainage Service Department (2008) *Flooding blackspots*. Drainage Services Department, Hong Kong
- Fan RL, Zhang LM, Wang HJ, Fan XM (2018) Evolution of debris flow activities in Gaojiagou ravine during 2008–2016 after the Wenchuan earthquake. *Eng Geol* 235:1–10
- FLO-2D Software Inc (2009) *FLO-2D Reference Manual*. Nutrioso, Arizona, U.S.A
- Fredlund DG, Morgenstern NR, Widger RA (1978) The shear strength of unsaturated soils. *Can Geotech J* 15(3):313–321
- Fredlund DG, Rahardjo H (1993) *Soil mechanics for unsaturated soils*. John Wiley & Sons, Inc, New York
- Fyfe JA, Shaw R, Compess SDG, Lai KW, Kirk PA (2000) *The quaternary geology of Hong Kong*. Geotechnical Engineering Office, Civil Engineering and Development Department, Hong Kong
- Gao L, Zhang LM, Chen HX (2015) Likely scenarios of natural terrain shallow slope failures on Hong Kong Island under extreme storms. *Nat Hazards Rev* 18(1):B4015001
- Gao L, Zhang LM, Chen HX, Shen P (2016) Simulating debris flow mobility in urban settings. *Eng Geol* 214:67–78
- Gardner WR (1958) Some steady-state solutions of the unsaturated moisture flow equation with application to evaporation from a water table. *Soil Sci* 85(4):228–232
- Geotechnical Control Office (1982) *Mid-levels study: report on geology, hydrology and soil properties*. Geotechnical Control Office, Hong Kong
- Han XD, Chen JP, Xu PH, Niu CC, Zhan JW (2018) Runout analysis of a potential debris flow in the Dongwopu gully based on a well-balanced numerical model over complex topography. *Bull Eng Geol Environ* 77(2):679–689
- Han Z, Li Y, Huang JL, Chen GQ, Xu LR, Tang C, Zhang H, Shang YH (2017) Numerical simulation for run-out extent of debris flow using an improved cellular automaton model. *Bull Eng Geol Environ* 76(3):961–974
- Hanson GJ, Simon A (2001) Erodibility of cohesive streambeds in the loess area of the midwestern USA. *Hydrol Process* 15(1):23–38
- He SM, Ouyang CJ, Liu W, Wang DP (2016) Coupled model of two-phase debris flow, sediment transport and morphological evolution. *Acta Geologica Sinica-English Edition* 90(6):2206–2215
- Huang Y, Cheng HL, Dai ZL, Xu Q, Liu F, Sawada K, Moriguchi S, Yashima A (2015) SPH-based numerical simulation of catastrophic debris flows after the 2008 Wenchuan earthquake. *Bull Eng Geol Environ* 74(4):1137–1151
- Hungr O (1995) A model for the runout analysis of rapid flow slides, debris flows, and avalanches. *Can Geotech J* 32:610–623
- Hungr O, McDougall S (2009) Two numerical models for landslide dynamic analysis. *Comput Geosci* 35(5):978–992
- Ho KKS (2013) Managing the uncertainties of natural terrain landslides and extreme rainfall in Hong Kong. *Landslide science and practice*: 285–302
- Julien PY, Lan Y (1991) Rheology of hyperconcentrations. *J Hydraul Eng* 117(3):346–353
- King JP (2013) *Tsing Shan Debris Flow and Debris Flood*, GEO Report No. 281. Geotechnical Engineering Office, Civil Engineering and Development Department, Hong Kong
- Ko FWY, Lo FLC (2016) Rainfall-based landslide susceptibility analysis for natural terrain in Hong Kong - a direct stock taking approach. *Eng Geol* 215:95–107
- Lam CLH, Lau JWC, Chan HW (2012) *Factual report on Hong Kong rainfall and landslides in 2008*, GEO Report No. 273. Geotechnical Engineering Office, Civil Engineering and Development Department, Hong Kong
- Li ACO, Lau JWC, Cheung LLK, Lam CLH (2009) *Review of landslides in 2008*, GEO Report No. 274. Geotechnical Engineering Office, Civil Engineering and Development Department, Hong Kong
- Li YM, Ma C, Wang YJ (2017) Landslides and debris flows caused by an extreme rainstorm on 21 July 2012 in mountains near Beijing, China. *Bull Eng Geol Environ* 3:1–16
- O'Brien JS, Julien PY (1988) Laboratory analysis of mudflow properties. *J Hydraul Eng* 114(8):877–887
- Ouyang C, He S, Tang C (2015) Numerical analysis of dynamics of debris flow over erodible beds in Wenchuan earthquake-induced area. *Eng Geol* 194:62–72
- Pudasaini SP (2012) A general two-phase debris flow model. *J Geophys Res: Earth Surf* 117:F03010
- Shen P, Zhang LM, Chen HX, Fan RL (2018) EDDA 2.0: integrated simulation of debris flow initiation and dynamics considering two initiation mechanisms. *Geosci Model Dev* 11(7):2841–2856
- Staley DM, Kean JW, Cannon SH, Schmidt KM, Laber JL (2013) Objective definition of rainfall intensity–duration thresholds for the initiation of post-fire debris flows in southern California. *Landslides* 10(5):547–562

- Takahashi T, Nakagawa H, Harada T, Yamashiki Y (1992) Routing debris flows with particle segregation. *J Hydraul Eng* 118(11):1490–1507
- World Meteorological Organization (2009) Manual on estimation of probable maximum precipitation (PMP). WMO-No. 1045, Geneva
- Zhang LL, Zhang J, Zhang LM, Tang WH (2011) Stability analysis of rainfall-induced slope failures: a review. *Geotech Eng Proc Instit Civ Eng* 164(5):299–316
- Zhang N, Matsushima T, Peng NB (2018) Numerical investigation of post-seismic debris flows in epicentral area of the Wenchuan earthquake. *Bull Eng Geol Environ*:1–16. <https://doi.org/10.1007/s10064-018-1359-6>
- Zhang S, Zhang LM (2017) Impact of the 2008 Wenchuan earthquake in China on subsequent long-term debris flow activities in the epicentral area. *Geomorphology* 276:86–103
- Zhang S, Zhang LM, Glade T (2014) Characteristics of earthquake- and rain-induced landslides near the epicentre of Wenchuan earthquake. *Eng Geol* 175:58–73
- Zhang S, Zhang LM, Chen HX, Yuan Q, Pan H (2013) Changes in runout distances of debris flows over time in the Wenchuan earthquake zone. *J Mt Sci* 10(2):281–292
- Zhu H, Zhang LM, Xiao T, Li XY (2017) Enhancement of slope stability by vegetation considering uncertainties in root distribution. *Comput Geotech* 85:84–89
- Zhu H, Zhang LM (2015) Evaluating suction profile in a vegetated slope considering uncertainty in evapotranspiration. *Comput Geotech* 63(1):112–120